CFD Models for Wall Shear Stress Estimation; a Comparative study of two Complete Scaffold Geometries

F. Maes, B. Van Baelen , P. Van Ransbeeck,
University College Ghent, Belgium

M. Moesen, H. Van Oosterwyck,
Katholieke Universiteit Leuven, Belgium

P. Verdonck
University Ghent, Belgium

ABSTRACT:

1 INTRODUCTION

Bone tissue engineering is a promising procedure to overcome the drawbacks of current bone replacing procedures (like allografts and autografts). Autologous osteoprecursor cells are seeded upon a support structure (scaffold) and cultured in vitro, in order to form a bone construct. One of the challenges is the formation of viable constructs of clinically relevant sizes. Large (>1cm) constructs often result in a necrotic central region with only a dense layer of cells at the construct periphery. The use of perfusion bioreactors in combination with macroporous scaffolds may improve mass transport and nutrient exchange during *in vitro* culture. Results indeed show an increase in cell viability and matrix formation compared to static controls [1, 2]. In addition, the culture media flow is known to influence osteogenesis through biophysical stimulation of the seeded bone precursor cells [3]. To get a better understanding of tissue formation in scaffolds it is therefore crucial to get more insight in the fluid dynamical environment in scaffolds.
However simulating flow fields and shear stresses exerted on the wall in irregular scaffolds are far from trivial. Several attempts focused on accurately modeling a subpart of an entire scaffold because of limitations in computer power. These sub models, although simulated correctly, suffer from important influences from the lateral boundaries. The only way to overcome this is modeling a complete geometry with a sufficient resolution.

2 MATERIALS AND METHODS

2.1 *Geometry Reconstruction*

A µCT scanner (HOMX 161 X-ray system with AEA Tomohawk CT-upgrade, Philips X-ray, Hamburg, Germany) was used to obtain images of both a titanium (Ti) and a hydroxyapatite (HA) scaffold with a voxel resolution of 8 µm. The threshold grey value was assigned by comparing material volume obtained from Archimedes measurements with the 3D volume calculated from the images through varying the threshold value in Tview (Skyscan, Kontich, Belgium).

2.2 *CFD model creation*

Democells, an in-house meshing program based on the CGAL C++ library [10], was used to create triangular surface meshes from micro-CT images of the entire scaffold. As a resolution of 8 µm would be computationally too expensive we coarsened the input images 5 times (6 times for Ti), and matched the element size accordingly, resulting in a maximum triangle circumdiameter of 40 µm (48µm for Ti). Corrections and adjustments have been performed using Mimics 13 (Materialise NV, Leuven, Belgium).
The resulting geometry consists of the void of the scaffold. To avoid forcing a predefined mass flow through the channels at the inlet we added a flow guidance in front of the inlet with a height of 0.5mm (Figuur 1). This way the flow itself will preferentially choose the channels with the least resistance, thus better mimicking realistic inlet conditions (Figure **1**). Starting from this surface mesh we used TGrid 5.0 (ANSYS, Inc., Lebanon, USA) to create a volume mesh of 25 000 000 elements for the HA scaffold and 17 000 000 elements for the Ti scaffold. A growth ratio of maximum 1.3 was used to gradually increase the 3D element size within the fluid volume in order to reduce the number of tetrahedral elements.
A flat velocity profile of 34 µm/s (corresponding to rate of 0.04 ml/min) through a circular area with a

diameter of 5 mm is imposed at the inlet. The lateral walls of the scaffolds are modeled as being embedded in a silicon tube. As scaffolds were not perfectly circular this was modeled as an elliptical cylinder (with almost no difference between the shortest and longest diameter) wrapped as tight as possible around the scaffold. To avoid side flow between the cylindrical wall and the scaffold some extremities of the scaffold were cut off enabling a closer wrapping of the cylinder (Figure **1** and Figure 3 (3D views)).
The culture medium was modeled as an incompressible and homogeneous Newtonian fluid with ρ = 1000 kg/m^3 and a measured dynamic viscosity of 8.51x10^{-4} Pa.s. Simulations are performed with Fluent 6.3 (ANSYS, Inc., Lebanon, USA). Calculations are done on a 16 CPU cluster with 64 GB RAM. Pre and post processing is done on an 8 CPU desktop with 24 GB RAM.

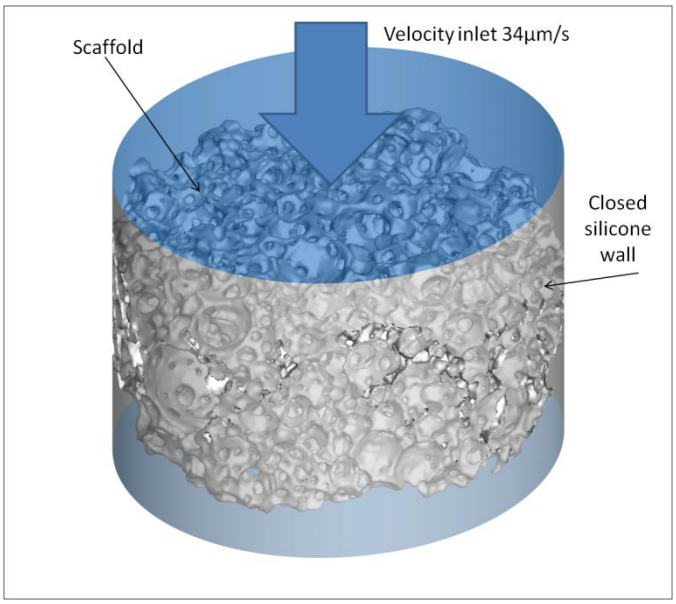

Figure 1: BC's adopted for the CFD calculations visualized on the HA scaffold. Velocity is based on 0.04 ml/min flow through a scaffold of 5 mm diameter. Flow direction is from top to bottom. Scaffold walls are colored light grey. Vertical cylindrical wall represents the silicone embedded around the scaffold. Openings in the wall occur when the scaffold makes contact with the silicone

3 RESULTS

The internal steady flow pattern is visualized with streamlines, color-coded according to the local velocity magnitude using Tecplot 360 (Tecplot, Inc. Bellevue, WA, USA). For both geometries the same color scale is used to enable comparison of the internal flow. Static pressure and WSS are visualized in combination with streamlines, color-coded according to velocity magnitude in order to link hydrodynamic parameters to each other.

3.1 *Titanium versus hydroxyapatite scaffold*

As seen from the plots in Figure 3, the streamlines show a highly tortuous behavior. The maximal velocity of the HA scaffold (1,1mm/s) is a little higher compared to the maximal velocity of the Ti scaffold (0,9mm/s). Accordingly, the maximal shear stress is of the same order of magnitude in both scaffolds (0.025 Pa for HA and 0.026 Pa for Ti). Surface averaged wall shear stresses however are much lower (0.00109 Pa for Ha and 0.00141 Pa for Ti). This is due to the highly skewed WSS distributions shown in Figure **2**.

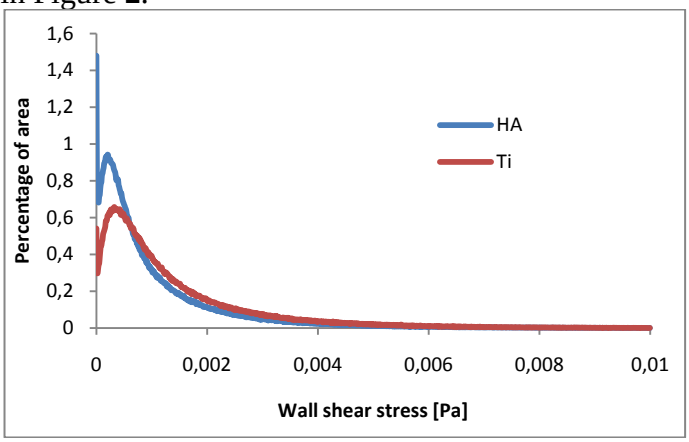

Figure 2: Histogram of WSS in hydroxyapatite (blue) and titanium (red). 1000 divisions are calculated and only the topline of the histogram is shown. The plot is truncated at 0.01Pa.

Top view of both scaffolds show zones with highly preferential flow paths for both scaffolds. These zones correspond to zones with low pressure (low resistance) and occur mostly at big pores being strongly interconnected. Looking closely one could also notice that the zones of high preferential flows lead to neighboring pores that have much less, almost zero, flow. Qualitatively one could say that this occurs more prominently at the inlet of the HA scaffold.

Considering the pressure at the wall a higher maximal value is noticed in the Ti scaffold (0.13 Pa versus 0.09 Pa for the HA scaffold). Since the same media flow rate is applied to both geometries this pressure difference is an indication of the resistance of the geometry. This higher resistance to fluid flow in the Ti scaffold corresponds to the higher prevalence of preferential flows in the HA scaffold.

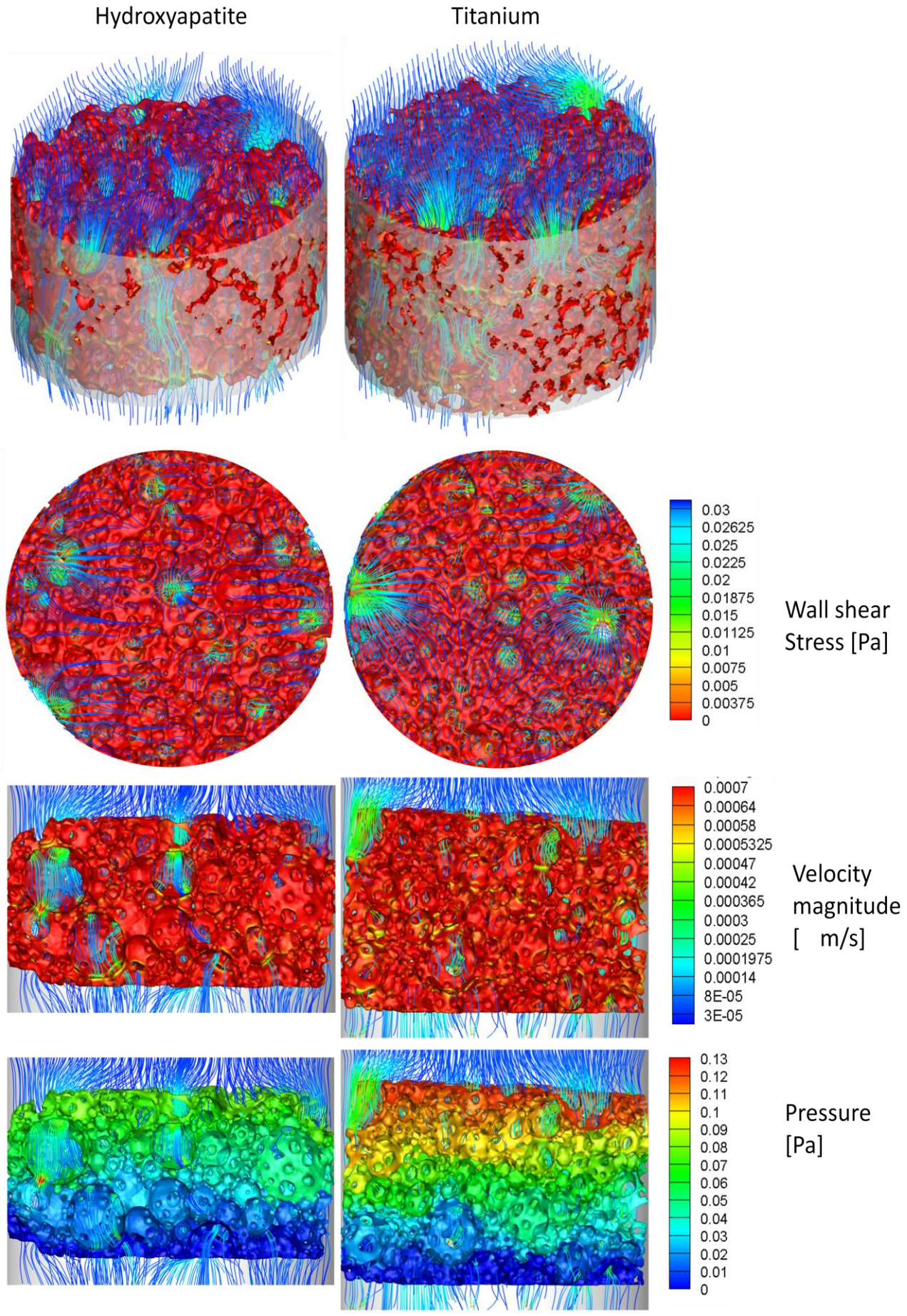

Figure 3. Visualization of the wall shear stress (WSS) and the static pressure (P) on the walls, all in combination with streamlines color-coded according to velocity magnitude. Flow is from top to bottom. The plots on the left show the results for titanium while the plots on the right are for hydroxyapatite. From top to bottom: 3D impression showing WSS, top view of the inlet (WSS), transversal cutplot showing the internal structure in the middle of the geometry (WSS), same cutplot but showing the pressure.

4 DISCUSSION

The aim of this study was to quantify the flow field through a titanium and a hydroxyapatite scaffold and to estimate the WSS imposed on the seeded cells. Depending on the value of WSS the proliferation and osteogenic differentiation of cells subjected to perfusion may be enhanced. As previously summarized in Maes et al. [4] a combination of in vitro culture perfusion results and numerical WSS estimations in irregular scaffolds is listed in Table 1.

Table 1. Critical WSS values for seeded cells in a scaffold subjected to culture media perfusion

WSS [mPa]	Effect	Author
1.5-13.5	Stimulation	Raimondi et al.[5]
0.05	Proliferation	Cartmell et al. [6]
1	Differentiation	
57	Apoptosis	
4.6	No effect	Raimondi et al. [7]
14-25	Differentiation	
56	Cell wash out	

Since the WSS estimations of the entire geometries are of the same order of magnitude as our previous simulations [4] the conclusions concerning a possible stimulating effect of WSS in the scaffolds considered here, are parallel. According to Cartmell et al. [6] the estimated WSS would enhance differentiation of the seeded cells, while Raimondi et al. [7] suggested that there would be no effect. Obviously, this needs to be confirmed by means of experiments with the scaffolds under investigation.

Table 2. Comparative table of WSS estimations adapted from Voronov et al. [8]

In Table 2 all reported WSS estimated with analogous inlet conditions are in the same order of magnitude as our results.

Of particular interest is the comparison with our previous study since they are performed using the same scaffold geometries. Because of computer limitations our previous study estimated WSS in cubic sub portions since simulating the complete scaffold was not feasible at that time. Of particular interest is the comparison with our previous study since both studies are performed using the same scaffold geometries (Table 3). Because of computer limitations our previous study estimated WSS in cubic sub portions of one twentieth of the volume since simulating the complete scaffold was not feasible at that time. Comparison shows that the results of the entire scaffold are very close to the results of the smaller 1mm cubic sub model (Table 3).

Both our studies tried to explore the variance inside scaffolds by calculating WSS in concentric sub regions of different sizes. A combination of these studies is depicted in Figure 4.

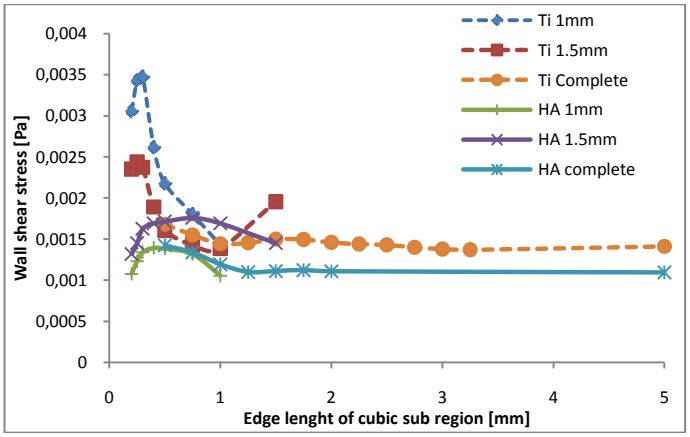

Figure 4: surface averaged wall shear stress for a number of regions of interest calculated in 3 CFD models created for both HA and Ti. Horizontal axis depicts the size of the region of interest expressed as edge length of the cubic portion. Last point of every line shows the WSS of the complete CFD model. Cubic regions of interest are exactly the same for the cubic sub models but are different than the regions in the complete model

reference	Scaffold type	Manufacturing method	CFD method	Flow rates mL/min	Number of samples	Domain size	WSS [Pa] average
Cioffi et al. [9]	Degrapol	Freeze-immersion-precipitation	Fluent	0,5 3 6 9	1 (3sub-volumes)	0,064mm³ relevant: 0,001mm³	0,00394 0,0241 0,04748 0,07135
Sandino et al. [10]	Calcium phosphate	Foaming albumen	Finite element Marc-Mentat	1,7 e-5 1,7 e-3	1	1,5mm³	0,04
Cioffi et al. [11]	Polyethylene glycol tetraphtalate	Compression modeling	Fluent	0,03 0,3	1	1,95mm³ cube	0,000256 0,00256
Maes et al. [4]	Titanium	gelcating	fluent	0,04	1 (5 ROI)	1-3,375mm³	0,0014 0,00195
	Hydroxyapatite				1 (5 ROI)		0,0011 0,00146
jungreuther-mayer et al.[12]	Collagen-glycosaminoglycan	lycophilization	OpenFOAM	1	1 (3 sub-volumes)	0.64³mm³ Relevant : 0.32mm³	0.2

Table 3. WSS estimations of present study compared to WSS estimations of previous study performend in the same scaffold geometries

Properties	**Present study**		**Previous study [4]**			
Material	Titanium	Hydroxya-patite	Titanium		Hydroxyapatite	
			Ti 1mm	Ti 1.5mm	HA 1mm	HA 1.5mm
Porosity	70 %					
Pore size	275 µm					
Element size	48µm	40µm	8 µm			
Modeled volume	79 mm³	68 mm³	1 mm³	3.375 mm³	1mm³	3.375 mm³
# elements	22 000 000	17 000 000	1 000 000	1 800 000	1 000 000	1 800 000
Inlet velocity	34 µm/s					
Average WSS	1.40 mPa	1.10 mPa	1.40 mPa	1.95 mPa	1.10 mPa	1.46 mPa

Figure 4 shows for Titanium a very good agreement between the 1.5 mm model and the complete model except when WSS is calculated for the entire model. The deviation of this last point can be explained by the effect of artificial boundary conditions imposed on the lateral wall of the sub model. Those lateral walls are modeled as closed where in reality media flow is passing through. The ideal distance from the boundaries is therefore 0.5/2 mm or approximately one pore size. The HA model however probably needs to be larger than 1.5 mm to account for the heterogeneity that induces the large preferential flow covering a prominent part of the smaller sub models.

The large preferential flow paths could compromise cell growth since a large amount of the culture medium is flowing through a comparably small part of the scaffold void. This causes mainly two effects: firstly there will be less nutrients and oxygen available for the cells, and secondly this disrupts the prevalence of a more uniform WSS distribution. This can also be extracted from the WSS histograms in Figure 2. There one notices that the WSS distribution of the HA scaffold is more skewed than that of the Ti scaffold. There is also a higher prevalence of surfaces where the shear stress is almost zero in the HA scaffold. Apparently there are more zones in the HA scaffold with virtually no flow at all resulting in less optimal cell culture conditions.

5 CONCLUSIONS

We were able to create CFD models of two complete scaffolds using boundary conditions closely matching reality and estimate wall shear stress with a high accuracy. Using these models in comparison with smaller sub models we could provide guidelines in model creation regarding size and dealing with wrongly closed lateral wall boundary conditions inherent to smaller sub models. These results should encourage further modeling of for example oxygen and nutrient uptake and cellular proliferation.

6 REFERENCES

1. Glowacki, J., S. Mizuno, and J.S. Greenberger, *Perfusion enhances functions of bone marrow stromal cells in three-dimensional culture.* Cell Transplantation, 1998. **7**(3): p. 319-326.
2. Bancroft, G.N., et al., *Fluid flow increases mineralized matrix deposition in 3D perfusion culture of marrow stromal osteloblasts in a dose-dependent manner.* Proceedings of the National Academy of Sciences of the United States of America, 2002. **99**(20): p. 12600-12605.
3. McGarry, J.G., et al., *A comparison of strain and fluid shear stress in stimulating bone cell responses - a computational and experimental study.* Faseb Journal, 2004. **18**(15): p. 482-+.

4. Maes, F., et al., *Modeling fluid flow through irregular scaffolds for perfusion bioreactors.* Biotechnol Bioeng, 2009. **103**(3): p. 621-30.
5. Raimondi, M.T., et al. *Integration of computational and experimental methods in the study of cartilage mechanobiology*. 2002.
6. Cartmell, S.H., et al., *Effects of medium perfusion rate on cell-seeded three-dimensional bone constructs in vitro.* Tissue Engineering, 2003. **9**(6): p. 1197-1203.
7. Raimondi, M.T., et al., *The effect of hydrodynamic shear on 3D engineered chondrocyte systems subject to direct perfusion.* Biorheology, 2006. **43**(3-4): p. 215-222.
8. Voronov, R., et al., *Computational modeling of flow-induced shear stresses within 3D salt-leached porous scaffolds imaged via micro-CT*. Journal of Biomechanics. **43**(7): p. 1279-1286.
9. Cioffi, M., et al., *Modeling evaluation of the fluid-dynamic microenvironment in tissue-engineered constructs: A micro-CT based model.* Biotechnology and Bioengineering, 2006. **93**(3): p. 500-510.
10. Sandino, C., J.A. Planell, and D. Lacroix, *A finite element study of mechanical stimuli in scaffolds for bone tissue engineering.* Journal of Biomechanics, 2008. **41**(5): p. 1005-1014.
11. Cioffi, M., et al., *Computational evaluation of oxygen and shear stress distributions in 3D perfusion culture systems: Macro-scale and micro-structured models.* Journal of Biomechanics, 2008. **41**(14): p. 2918-2925.
12. Jungreuthmayer, C., et al., *A Comparative Study of Shear Stresses in Collagen-Glycosaminoglycan and Calcium Phosphate Scaffolds in Bone Tissue-Engineering Bioreactors.* Tissue Engineering Part A, 2009. **15**(5): p. 1141-1149.
13. CGAL Computational Geometry Algorithms Library http://www.cgal.org